

Phase transitions and entanglement properties in spin-1 Heisenberg clusters with single ion anisotropy

V. S. Abgaryan¹, N. S. Ananikian¹, L. N. Ananikyan¹ and A. N. Kocharian^{1,2}

¹ Alikhanyan National Science Laboratory, Alikhanian Br. 2, 0036 Yerevan, Armenia

² Department of Physics, California State University, Los Angeles, CA 90032, USA

E-mail: ananik@yerphi.am

Abstract. The incipient quantum phase transitions of relevance to non-zero fluctuations and entanglement are studied in Heisenberg clusters by exploiting the negativity as a measure in bipartite and frustrated spin-1 anisotropic Heisenberg clusters with bilinear-biquadratic exchange, single-ion anisotropy and magnetic field. Using exact diagonalization technique it is shown that quantum critical points signaled by qualitative changes in behavior of magnetization and particle number, is ultimately related to microscopic entanglement and collective excitations. The plateaus and peaks in spin and particle susceptibilities, define the conditions for a high/low density quantum entanglement and various ordered phases with different spin (particle) concentrations.

PACS numbers: 75.10.Jm, 75.10.Dg, 03.67.-a, 64.70.-p, 37.10.Jk

1. Introduction

Entanglement properties for few spins or electrons can display the general features of large thermodynamic systems and different measures of entanglement have been defined to understand QPTs [1, 2]. A finite spin system is important in the context of molecular magnetism and spin pairing. A new line of research points to a connection between the local entanglement in one-dimensional correlated systems and the existence of a QPTs and scaling [4, 5] relevant to the quantum critical points (QCPs). Furthermore, such a connection can be exploited to unveil a fundamental connection between the QCPs in finite-size small, large clusters [6, 7] and macroscopic systems [2]. A particle and spin density fluctuations, extending the essential properties of entanglement beyond the conventional framework, have been introduced with the explicit reference to the phase transitions in canonical and grand canonical ensembles signaled by a critical behavior in terms of the energy gaps and susceptibilities [8, 9]. The quantum gas of clusters at the equilibrium gives unprecedented opportunity to explore exactly these ideas for a quantum dynamics of spin fluctuations [10]. While the basic features of entanglement in spin- $\frac{1}{2}$ systems are by now fairly well understood [11], entanglement properties of larger spin fermions (or bosons) are less known due to the lack of good operational measures for high spin entanglement [12]. A general classical spin-1 Blume-Emery-Griffiths (BEG) model [13] has proven to be a useful for description of liquid-gas, liquid-crystal phase transitions, tricritical and λ points, spontaneous phase separation [14, 15, 16, 17]. The integer spin Heisenberg model exhibits a characteristic spin gap and very rich phase diagrams [18, 19]. Exact calculations of thermodynamic and entanglement properties in finite-size clusters can give an appealing alternative to get insight into the general features of bipartite and frustrated systems [20]. Some analytical and numerical studies of entanglement and negativity in bilinear-biquadratic spin-1 Heisenberg model on dimerized bipartite and frustrated systems have been performed in [22, 23, 24, 25]. The entanglement with bilinear-biquadratic Hamiltonian has been considered for the case of two spins (qubit) in the absence of crystal field [26]. One of interesting problems concerning entanglement is to study the effect of uniaxial single-ion anisotropy and magnetic fields on negativity. An exact calculation of entanglement versus longitudinal crystal field and biquadratic coupling for analyzing the variation of negativity versus parameters of the spin-1 system have not been attempted either for ferromagnetic or antiferromagnetic Heisenberg model even for small bipartite and frustrated clusters. The aim of this work is to discuss, in a general framework, how microscopic entanglement in the two- and three-qubit context can be related to a QCPs characterized by plateaus in peak behavior of the spin revealed in saddle point singularities on model parameters. We provide a reinterpretation of the spin and particle susceptibilities near quantum critical points in terms of the quantum entanglement in a physically transparent way. Here we adopt negativity to measure the ground state entanglement for spin-1 systems, to reveal QPTs in terms of negativity. We have two main goals in this paper: The first is to provide a global view of the most general spin-1 Heisenberg model which have not been

highlighted so far in minimal clusters. The second is to show that quantum entanglement exhibits the existence of characteristic plateaus in negativity related to QPTs. In this paper we perform exact calculations of entanglement and response functions in spin-1 Heisenberg model with bilinear-biquadratic exchange interactions in longitudinal crystal and magnetic fields. The basic principles for calculation of negativity are introduced in Sect. 3. The ground state magnetic and entanglement properties in spin-1 Heisenberg model for ferromagnetic and antiferromagnetic couplings are given in Sect. 4.1. The negativity analyzes in absence and presence of magnetic field are given in Sect. 4.2 and Sect. 4.3 respectively. The effect of nonlinear interaction is studied in Sect. 4.4). Results for frustrated trimer are presented in Sect. 4.5. The conclusion is given in Sect. 5.

2. Spin-1 Heisenberg model

We consider the spin-1 isotropic Heisenberg model in the presence of magnetic field $B < 0$

$$H = \sum_{i=1}^N [J(\vec{S}_i \vec{S}_{i+1}) + K(\vec{S}_i \vec{S}_{i+1})^2] + D \sum_{i=1}^N (S_i^z)^2 + B \sum_{i=1}^N S_i^z. \quad (1)$$

The linear J and nonlinear K terms are the exchange and quadrupolar interactions. Here we implemented the longitudinal crystal field D , which describes an uniaxial single-ion anisotropy. In what follows, the crystal field significantly changes the results on the entanglement. Notice, effective spin Hamiltonian (2) can be derived from Bose-Hubbard model in the strong coupling limit. The local spin vector \vec{S}_i for each site has components of the Spin-1 operators

$$S_x = \frac{1}{\sqrt{2}} \begin{pmatrix} 0 & 1 & 0 \\ 1 & 0 & 1 \\ 0 & 1 & 0 \end{pmatrix}, S_y = \frac{1}{\sqrt{2}} \begin{pmatrix} 0 & -i & 0 \\ i & 0 & -i \\ 0 & i & 0 \end{pmatrix}, \\ S_z = \begin{pmatrix} 1 & 0 & 0 \\ 0 & 0 & 0 \\ 0 & 0 & -1 \end{pmatrix}. \quad (2)$$

Unless otherwise specified, we will consider periodic boundary conditions, such that $\vec{S}_{N+1} = \vec{S}_1$, where N is the total number of lattice sites. The sum over lattice sites for crystal field term with $(S_i^z)^2$ in (2) can be reduced to the spin concentration (particle number),

$$\sum_{i=1}^N (S_i^z)^2 = P - P_0,$$

where P_0 the number of lattice sites with $S_i^z = 0$. Notice, the axial anisotropy in many respects is analogous to the chemical potential $D = -\mu$.

3. Definitions and Basic

At thermal equilibrium, the state of the system is determined by the density matrix

$$\hat{\rho}(T) = \frac{e^{-\frac{H}{k_B T}}}{Z} = \sum_i \frac{e^{-\frac{E_i}{k_B T}}}{Z} |\psi_i\rangle \langle \psi_i|, \quad (3)$$

where E_i are the eigenvalue of the i -th quantum many body eigenstate and the partition function is $Z = \sum_i e^{-\beta E_i}$ with $\beta = 1/k_B T$ ($k_B = 1$). The many-body entanglement is described by the density operator in [20, 27, 28, 29]. For spin-1 system the degree of pairwise entanglement, measured in terms of the negativity Ne , can be employed to evaluate the thermal state of concern [30]. The negativity of a state ρ is defined as

$$Ne = \sum_i |\mu_i|, \quad (4)$$

where μ_i 's are negative eigenvalues of ρ^{T_1} and T_1 denotes the the partial pairwise transpose with respect to the first system, i.e., for bipartite system in state ρ it is defined as

$$\langle i_1, j_2 | \rho^{T_1} | k_1, l_2 \rangle \equiv \langle k_1, j_2 | \rho | i_1, l_2 \rangle, \quad (5)$$

for any orthonormal but fixed basis. Definition (4) is equivalent to

$$Ne = \frac{\|\rho^{T_1}\|_1 - 1}{2}, \quad (6)$$

where $\|\rho^{T_1}\|_1$ is trace norm of ρ ($\rho = Tr \sqrt{\rho^\dagger \rho}$). For unentangled states negativity vanishes, while $Ne > 0$ gives a computable measure of thermal entanglement.

As thermodynamical characterisation we have used the responses of the thermodynamical potential with respect to D and B which are follows

$$P = \langle (S^z)^2 \rangle = \frac{\partial F}{\partial D}, \quad \langle S^z \rangle = \frac{\partial F}{\partial B}. \quad (7)$$

Here F is the free energy $F = -T \ln Z$ and $\langle \dots \rangle$ indicates averaging performed within a canonical ensemble. The responses for the first derivatives of the thermodynamic potential with respect to D and B provide exact expressions for particle χ_D and spin χ_B susceptibilities:

$$\chi_D = \frac{\partial P}{\partial D}, \quad \chi_B = \frac{\partial \langle S^z \rangle}{\partial B} \quad (8)$$

4. Results

4.1. Entanglement and magnetic properties of spin-1 isotropic Heisenberg dimer

In this section, we consider Hamiltonian in case of $N = 2$, namely Heisenberg model. In the two-qubit case, we diagonalize the Hamiltonian, and obtain the eigenvalues

$$\begin{aligned}
 E_1 &= -2(B - J - K - D), & E_2 &= -2(J - K - D), \\
 E_3 &= 2(B + J + K + D), & E_4 &= -B - 2J + 2K + D, \\
 E_5 &= B - 2J + 2K + D, & E_6 &= -B + 2J + 2K + D, \\
 E_7 &= B + 2J + 2K + D, & E_8 &= -J + 5K + D - \lambda_0 \\
 E_9 &= -J + 5K + D + \lambda_0,
 \end{aligned} \tag{9}$$

and corresponding eigenvectors

$$\begin{aligned}
 |\psi_1\rangle &= |-1, -1\rangle, & |\psi_2\rangle &= \frac{1}{\sqrt{2}}(|-1, 1\rangle - |1, -1\rangle), \\
 |\psi_3\rangle &= |1, 1\rangle, & |\psi_4\rangle &= \frac{1}{\sqrt{2}}(|-1, 0\rangle - |0, -1\rangle), \\
 |\psi_5\rangle &= \frac{1}{\sqrt{2}}(|0, 1\rangle - |1, 0\rangle), & |\psi_6\rangle &= \frac{1}{\sqrt{2}}(|-1, 0\rangle + |0, -1\rangle), \\
 |\psi_7\rangle &= \frac{1}{\sqrt{2}}(|0, 1\rangle + |1, 0\rangle), \\
 |\psi_8\rangle &= \frac{1}{\sqrt{2 + \lambda_1^2}}(|1, -1\rangle + \lambda_1|0, 0\rangle + |-1, 1\rangle), \\
 |\psi_9\rangle &= \frac{1}{\sqrt{2 + \lambda_2^2}}(|1, -1\rangle + \lambda_2|0, 0\rangle + |-1, 1\rangle)
 \end{aligned} \tag{10}$$

where, $\lambda_0 = \sqrt{9(J - K)^2 - 2(J - K)D + D^2}$, $\lambda_1 = \frac{J - K - D - \lambda_0}{2(J - K)}$, $\lambda_2 = \frac{J - K - D + \lambda_0}{2(J - K)}$, and $|i, j\rangle$ ($i = -1, 0, 1$ and $j = -1, 0, 1$) are the eigenvectors of $S_i^z S_{i+1}^z$. According to Schmidt theorem $|\psi_5\rangle$ and $|\psi_7\rangle$ are not entangled and the maximum entangled states can be only $|\psi_8\rangle$ or $|\psi_9\rangle$. The partial transpose density matrix of the thermal state $\rho(T)$ at equilibrium is

$$\rho^{T_1} = \frac{1}{Z} \begin{pmatrix} \omega^- & 0 & 0 & 0 & \chi^- & 0 & 0 & 0 & \Xi^- \\ 0 & \chi^+ & 0 & 0 & 0 & \Omega & 0 & 0 & 0 \\ 0 & 0 & \Xi^+ & 0 & 0 & 0 & 0 & 0 & 0 \\ 0 & 0 & 0 & \chi^+ & 0 & 0 & 0 & \Omega & 0 \\ \chi^- & 0 & 0 & 0 & \Lambda & 0 & 0 & 0 & \zeta^- \\ 0 & \Omega & 0 & 0 & 0 & \zeta^+ & 0 & 0 & 0 \\ 0 & 0 & 0 & 0 & 0 & 0 & \Xi^+ & 0 & 0 \\ 0 & 0 & 0 & \Omega & 0 & 0 & 0 & \zeta^+ & 0 \\ \Xi^- & 0 & 0 & 0 & \zeta^- & 0 & 0 & 0 & \omega^+ \end{pmatrix}, \tag{11}$$

where

$$\omega^\pm = e^{\frac{2(\pm B - D - J - K)}{T}}, \quad \chi^\pm = \frac{1}{2} e^{-\frac{B + 2(J + K) + D}{T}} \left(1 \pm e^{\frac{4J}{T}} \right),$$

$$\begin{aligned}\zeta^\pm &= \frac{1}{2} e^{\frac{B-2(J+K)-D}{T}} \left(1 \pm e^{\frac{4J}{T}} \right), \\ \Xi^\pm &= \pm \frac{1}{2} e^{\frac{2(J-D-K)}{T}} + \\ &\quad \frac{e^{\frac{J-5K-D}{T}} (\lambda_0 \cosh \frac{\lambda_0}{T} + (J-K-D) \sinh \frac{\lambda_0}{T})}{2\lambda_0}, \\ \Omega &= \frac{2e^{\frac{J-5K-D}{T}} (K-J) \sinh \frac{\lambda_0}{T}}{\lambda_0}, \\ \Lambda &= \frac{e^{\frac{J-5K-D}{T}} (\lambda_0 \cosh \frac{\lambda_0}{T} - (J-K-D) \sinh \frac{\lambda_0}{T})}{\lambda_0},\end{aligned}$$

here the partition function is

$$\begin{aligned}Z &= e^{-\frac{2(D+J)+5K}{T}} \left(2e^{\frac{D+3K}{T}} (1 + e^{\frac{4J}{T}}) \cosh\left(\frac{B}{T}\right) + \right. \\ &\quad \left. e^{\frac{4J+3K}{T}} + 2e^{\frac{3K}{T}} \cosh\left(\frac{2B}{T}\right) + 2e^{\frac{D+3J}{T}} \cosh\left(\frac{\lambda_0}{T}\right) \right).\end{aligned}$$

4.2. Spin-1 in zero magnetic field

Here we analyze the effects of crystal field on the ground state entanglement in the spin-1 Heisenberg model (2) at zero field ($B = 0$). The (quadrupole) particle number and negativity plots in figures 1 a and b are both asymmetric as function of D for ferro $J > 0$ and antiferromagnetic $J < 0$ couplings. The monotonic behavior of P versus D in figure 1 a signals a smooth character of the phase transition. Note that this smooth bosonic behavior of spin concentration P versus D is contrasted from the (step-like) abrupt fermionic change in the electron number as a function of the chemical potential in [7]. At infinitesimal $T \rightarrow 0$ the variation of negativity figure 1b versus D for antiferromagnetic case ($J > 0$) is non monotonic. So, for $D = 0$, we have a highest possible entanglement and ψ_8 is a ground state of the system. The system for $J < 0$ displays two distinct phases: one separable and other entangled. For positive D region the negativity for $J > 0$ is more than for $J < 0$. For $D = 0$ the ground state is five fold degenerate (i.e., it is a mixture of $\psi_1, \psi_3, \psi_6, \psi_7, \psi_8$ states) with zero negativity. At infinitesimal $D \rightarrow +0$ the system is entangled in the pure state, ψ_8 . For $D < 0$ the ground state at $J < 0$ is double degenerate with a mixture of ψ_1 and ψ_3 states.

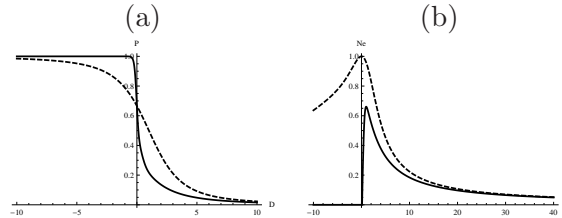


Figure 1. The density variation of a) the particle number P and b) the negativity Ne versus D for antiferromagnetic, $J = 1$ (dashed) and ferromagnetic, $J = -1$ (solid) cases

Notice, these states are separable (can be factorized), and therefore, according to definition, these quantum states are without entanglement. Thus, the entanglement in $D < 0$ region can be used to detect quantum correlations in antiferromagnetic case, which are absent for “classical” ferromagnetic.

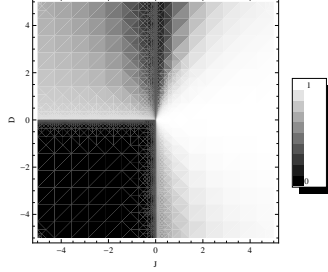


Figure 2. The density of negativity Ne versus of J and D . The crystal field D enhances the entanglement at $J < 0$.

The negativity is non monotonous function with one maxima at $D = 0$ for $J > 0$ and in a close vicinity to origin at $J < 0$. The magnetic and quadrupole susceptibilities, i.e $\chi_B \chi_D$, allows to distinguish the ordered and disordered phases in the case of broken-symmetry at QPTs. Figure 2 shows the pure (extremal) and mixed (non-extremal) quantum states. Disentangled dark region in ferromagnetic case corresponds to the plateau-like behavior in zero (spin) magnetic susceptibility $\chi_0 = \frac{\partial \langle s^z \rangle}{\partial h} |_{B \rightarrow 0}$ versus J and D plane in figure 3 a at $J < 0$.

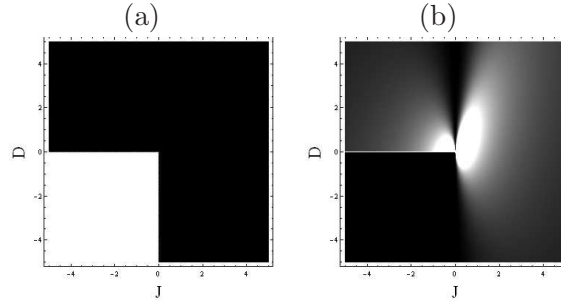


Figure 3. The densities for a) zero field (magnetic) spin susceptibility and b) particle susceptibility versus J and D .

The high density magnetic (spin) susceptibility in white sector corresponds to the low density of negativity in figure 2. The strong enhancement of negativity along the line $D = 0$ is relevant to the observed peaks in the particle susceptibility, $\chi_D = \frac{\partial \langle (S^z)^2 \rangle}{\partial D}$ in figure 3 a. The various regions seen for (density) negativity in figure 2 are reproduced in density of quadrupole susceptibility in figure 3 b versus D and J . Similarly, the phase diagram in $K - J$ space in the absence of D and B fields shows the degree of entanglement and phases due to effect of nonlinearity on the eigenvalues and eigenvectors in (10). For example, the $J = K$ line separates the maximum entangled and non-entangled phases for ferromagnetic coupling, while the $J = 3K$ line is a boarder between entangled and new less-entangled phases for antiferromagnetic coupling.

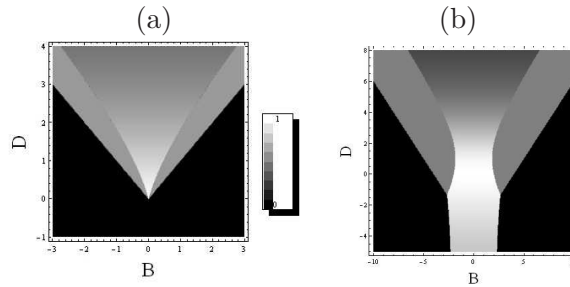


Figure 4. The density plot for negativity dependencies on crystal D and magnetic B fields at $T = 0$ for (a) $J = -1$ and (b) $J = 1$. For both (antiferromagnetic and ferromagnetic) cases there are more than three phases, which indicates the possible existence of triple or tricritical points.

We find that for $K > 0$, the line $J = 0$ as before separates non entangled and maximum entangled phases. The maximum entanglement, which exists for $J < 0$ at $K < J$ and for $J > 0$ at $J > 3K$, corresponds to observed condition for bose condensation of unpolarized Na atoms on optical lattice [21].

4.3. Effects of magnetic field

Magnetic field B partially removes the ground state degeneracy and in figure 4 one can see the presence of new phase boundaries. The entanglement properties of the excited states are independent from those in the ground states. Also we found that the pairwise entanglement decreases from ground state to excited states, i.e., the more excited the system, the less the entanglement. In ferromagnetic case for $D = 0$ and $B = 0$ point there is a maximum entangled state. In figures 4 a for $J = -1$ and 4 b for $J = 1$, the energies are measured with respect to $|J|$, which is set to 1. When $D < |B|$ the system is in ψ_1 or ψ_3 state, which is non-entangled. For fixed B the two consecutive phase transitions take place by increasing D at $D = |B|$ and $D = \sqrt{1 + 6|B| + B^2} - 1$, into ψ_6 and ψ_8 ground states correspondingly. For antiferromagnetic case, the phase diagram is more complex. The negativity contains the triple point at $|B| = \frac{8}{3}$ and $D = -\frac{4}{3}$, which implies the presence of various phases, possible coexistence or phase separation in spin-1 system. When $D < -\frac{4}{3}$, the line $|B| = -\frac{2}{-2+|B|} - 1$ separates ψ_8 and $\psi_{1,4}$, i.e. maximum entangled phase from non-entangled one. For $D > -\frac{4}{3}$ there are three phases in the ground state: non-entangled state at $D < |B| - 4$; the maximum entangled between $1 + \sqrt{B^2 + 2|B| - 7}$ and $1 - \sqrt{B^2 + 2|B| - 7}$; non saturated entanglement for $\psi_{4,5}$ states. In figure 4 there is no any entanglement beyond some critical field B_c restricting the black region. Also note that entanglement increases with D . Positive D values favor to the larger entanglement, while $D < 0$ shows the tendency toward non-entangled states with larger total spin. The ground state diagrams figures 2, and 4 exhibit quantum critical behavior on the borderlines between various states with continuously-varying quantum critical points separating antiferromagnetically ordered distinct phases from from the non-entangled state (spin liquid phase). These critical lines, similar to continues QCPs, can be used for the classification of the many-body ground states

of interacting spins and quadrupole moment in multidimensional parameter space. Dynamic interactions between the spins strongly renormalize various parameters in the effective Hamiltonian and, therefore, spin and quadrupole momentum have properties different from a quasiparticle description. As in QCP [2], various states along quantum critical boundaries here are necessarily separated by second order phase transitions with various entanglement and susceptibility. The quantum critical (lines) boundaries appear to be useful for understanding the formation of various thermodynamic phases in the ground state. These continuous boundaries in thermodynamic phase diagram at infinitesimal temperature coincide with the corresponding QCPs, derived from the peaks of magnetic susceptibilities in agreement with our preliminary analysis (see also [9, 8]). The boundaries between the various phases are useful for understanding also the behavior of thermal negativity for departure to non-zero temperatures.

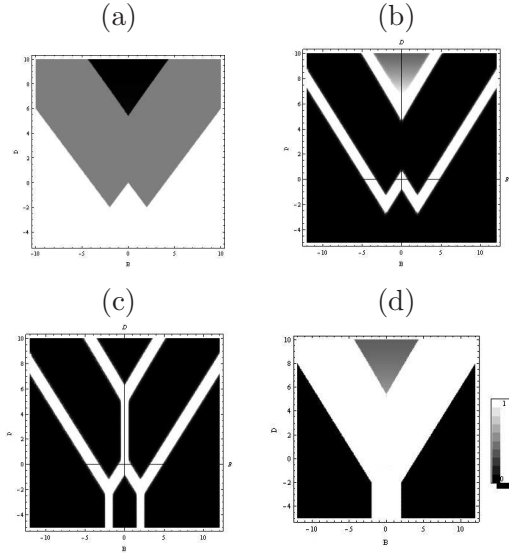


Figure 5. The density plots for (a) particle number P (b) (quadrupole) particle susceptibility (c) magnetic susceptibility and (d) negativity versus B and D when $K = 2$ in antiferromagnetic case $J = 1$.

The distances along the magnetic field in figures 4 between various phases define the stable magnetic phases with distinct spin gaps configurations, characterized by different spin concentration and diverging susceptibilities along the boundaries. For example, the negativity for white areas reaches the maximum (saturated) value, while there are also different distinct areas with partial (unsaturated) entanglement.

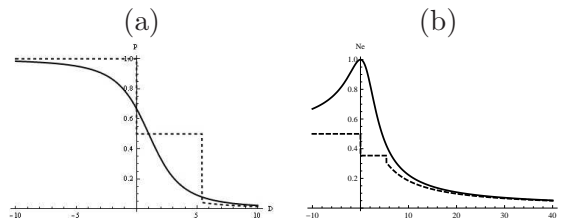


Figure 6. The density variation of a) particle number P and b) negativity Ne versus D for $K = 0$ (solid) and $K = 2$ (dashed) for antiferromagnetic ($J = 1$)

in zero field $B = 0$.

These density plots can be used to determine of QCPs and the boundaries for various QPTs. This result for finite size clusters can have important consequences in the physics of quantum phase transitions [2], where so far the usual method to detect a phase transition is to look at the scaling in the thermodynamic systems. The competition among the different phases can lead to complex behavior with the two triple points. The density of negativity is an efficient indicator of QPTs. In figure 5(a) we find the new spin phase boundaries from black to grey region with jump $\frac{1}{2}$ and from grey region into the two white ones with the same jump. The white middle line $B = 0$ in figure 5(c) corresponds to classical effect at $J < 0$ case (without change in entanglement). On the other hand, the continuous lines seen in the same plot at $J > 0$ correspond to quantum phase transitions (observable also in negativity).

4.4. Effect of quadruple term

Here we display effect of nonlinear interactions between the spins. The variation P versus D is shown in figure 6a for two quadruple interactions $K > 0$ for antiferromagnetic case with $J = 1$. At $K = 2$, an opposite spin pairing gap is opened at $P = 1/2$. Such a density profile, showing finite leap near $P = 1/2$, resembles the MH plateau behavior for the number of particles versus chemical potential in the Hubbard clusters. This is indicative of a possible opposite spin pairing instability [7]. Therefore, the cluster behaves at large K as a MH like insulator in contrast to the spin liquid like behavior with the zero gap, shown at $K = 0$ in figure 6b. As it is seen from the density plot the magnetic field and quadrupole interaction (K) makes the phase structure in antiferromagnetic case more richer. Our analysis shows that the negativity in $D - K$ space for ferromagnetic coupling is always less than for antiferromagnetic case.

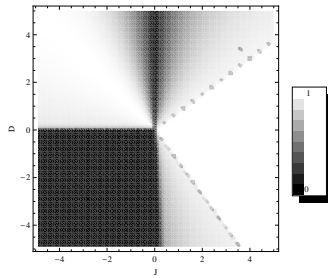


Figure 7. Density plot of negativity via J and D at $K = B = 0$ in three-sites cluster.

4.5. Non-bipartite clusters

Finally, we display in this session the results of negativity versus D and J for frustrated three-site clusters in figure 7 at rather low $T = 0.01$. This picture for ferromagnetic case resembles corresponding figure 2. However, there is an apparent difference in behavior for the region $J > 0$, where there are two extra continuous boarder lines.

5. Conclusion

In this paper we adopted the concept of entanglement to analyze behavior of the small-size spin-1 Heisenberg clusters. We used a negativity as a computable measure of entanglement to perform extensive calculations of the negativity and response functions. The critical fields and intrinsic parameters beyond which entanglement disappears are calculated. We found regions where the quantum entanglement can be increased more rapidly by increasing both, D and K . The negativity can determine the borders between ordered phases with excess correlations, above the classical ones. The observed plateaus and peaks in spin and particle behavior and susceptibilities can be considered as a possible universal method for the simultaneous detection of quantum and classical phase transitions. The (density) plots are convenient (topographic map) tool for observation of the quantum phases and quantum transitions. The states with vanishing classical correlations but existing quantum correlations in entanglement open up the new opportunities of phase transitions that are detectable only through correlation in behavior of entanglement and thermodynamic properties. Our studies of QCPs in small size spin clusters appear to be generic to large thermodynamic systems. The exact diagonalization is completely unbiased for the study of QPTs and QCPs in strongly correlated spin and electron systems [8]. Although the exact studies have limitations (since the computations grow exponentially with cluster size), we do not find a minimal critical length in clusters below which a quantum critical behavior disappears. The spin-1 boson Hubbard like model at certain conditions can be mapped onto the spin-1 Heisenberg model. Then these studies can also be useful for the analysis of spontaneous phase separation and the transition from Mott insulator to quantum superfluid in spin-1 BoseHubbard models on optical lattices.

Acknowledgments

We thank H Babujian for useful discussions. This work was supported by ANSEF 2497-PS, 1981-PS and ECSP-09-08 and NFSAT research grants. LA thanks S Wimberger for helpful discussion and acknowledges financial support from the EMMI through a grant within the Institute of Theoretical Physics of the University of Heidelberg, the Excellence Initiative of the DFG through the Heidelberg Graduate School of Fundamental Physics (grant number GSC 129/1). ANK thanks Edward Rezayi, Jose Rodriguez and Oscar Bernal for helpful discussions.

References

- [1] Amico L, Fazio R, Osterloh A and Vedral V 2008 *Rev. Mod. Phys.* **80**, 517; Horodecki R et al. 2009 *Rev. Mod. Phys.* **81** 865; Güühne O and Toth G 2009 *Phys. Rep.* **474** 1.
- [2] Sachdev S 1999 *Quantum Phase Transitions* (Cambridge University Press, Cambridge, England).
- [3] Sadler L E, Higbie J M, Leslie S R, Vengalattore M and Stamper-Kurn D M 2006 *Nature (London)* **443**,312.

- [4] Larsson D and Johannesson H 2005 *Phys. Rev. Lett.* **95**, 196406.
- [5] Yang C, Kocharian A N and Chiang Y L 2000 *J. Phys.: Condens. Matter* **12**, 7433.
- [6] Nagaoka Y 1966 *Phys. Rev.* **147**, 392
- [7] Kocharian A N et al. 2006 *Phys. Rev.* **B74**, 024511;
- [8] Kocharian A N et al. 2008 *Phys. Rev.* **B78**, 075431.
- [9] Kocharian A N et al. 2009 *Phys. Lett.* **A373**, 1074.
- [10] Leibfried D et al. 2005 *Nature (London)* **438**, 639.
- [11] Wootters W K 1998 *Phys. Rev. Lett.* **98**, 2245; Wang X et al. 2001 *J. of Physics A: Math. and Gen.* **34**, 11307; Ananikian N S , Ananikyan L N, Chakhmakhchyan L A and Kocharian A N 2011 *J. Phys. A: Math. Theor.* **44** 025001.
- [12] Mintert M et al. 2004 *Phys. Rev. Lett.* **92**, 167902.
- [13] Blume M, Emery V J and Griffiths R B 1971 *Phys. Rev.* **A4**, 1071.
- [14] Wong A P Y and Chan M W H 1990 *Phys. Rev. Lett.* **65** 2567.
- [15] Bellini T et al. 1992 *Phys. Rev. Lett.* **69**, 788.
- [16] Wu X N and Wu F Y 1986 *J. Stat. Phys.* **50**, 41; Horiguchi T 1986 *Phys. Lett.* **A113**,425.
- [17] Ananikian N S ,Avakian A R and Izmailyan N Sh 1991 *Physica A* **172**, 391; Akheyan A Z and Ananikian N S 1996 *J. Phys.* **A29**, 721.
- [18] Takhtajan L 1982 *Phys. Lett.* **A87**, 479; Babujan H 1983 *Nucl. Phys.* **B215**, 317.
- [19] Haldane F D M 1983 *Phys. Lett.* **A93**, 464.
- [20] Arnesen M C, Bose S and Vedral V 2001 *Phys. Rev. Lett.* **87**, 017901.
- [21] Stenger J et al 1998 *Nature (London)* **396**, 345.
- [22] Schollwöck U et al. 1996 *Phys. Rev.* **B53**, 3304.
- [23] Sun Z, Wang X and Li Y Q 2005 *New J. of Phys.* **7**, 83.
- [24] Zhang G F and Li S S 2006 *Solid State Commun.* **138**, 17.
- [25] Li D C et al. 2008 *J. Phys.: Condens. Matter* **20**, 325229.
- [26] Zhou L, Yi X X, Song H S and Quo Y Q 2003 (arXiv:quant-ph/0310169v2).
- [27] Wang X, Fu H and Solomon A I 2001 *J. Phys.* **A34**, 11307.
- [28] Schliemann J et al. 2001 *Phys. Rev.* **A64**, 022303.
- [29] Dür W et al. 2001 *Phys. Rev.* **A62**, 062314.
- [30] Vidal G and Werner R W 2002 *Phys. Rev.* **A65**, 032314.